Available online at www.sciencedirect.com
ScienceDirect
Surface & Coatings Technology 202 (2008) 2690–2697
SURFACE & COATINGS TECHNOLOGY
www.elsevier.com/locate/surfcoat

Solution-based synthesis of oxide thin films via a layer-by-layer deposition method: Feasibility and a phenomenological film growth model

Pavan K. Arcot, Jian Luo *

School of Materials Science and Engineering; Center for Optical Materials Science and Engineering Technologies, Clemson University, Clemson, SC 29634, USA

Received 17 June 2007; accepted in revised form 27 September 2007
Available online 4 October 2007

Abstract

The feasibility and kinetics of a generic layer-by-layer thin film deposition method are investigated using Y_2O_3-doped ZrO_2, pure ZrO_2, and Gd_2O_3-doped CeO_2 as model systems. Uniform nanocrystalline films have been made via dipping substrates alternately in cationic and anionic precursor solutions. The effects of several key processing parameters, including the number of deposition cycles, cationic concentration, dipping speed, and holding/immersing time, have been investigated. Growth rates of ~4–12 nm per deposition cycle for as-deposited films (i.e., ~2–6 nm/cycle for annealed films), tunable via varying the key deposition parameters, have been demonstrated.

Keywords: Chemical solution deposition; Sol gel; Growth models; Oxides; Zirconium Oxide; Layer-by-layer deposition

1. Introduction

A layer-by-layer deposition method has been widely applied to make polyelectrolyte thin films [1]. In this technique, substrates are alternately dipped into polycation and polyanion solutions to form polyelectrolyte multilayer films. Analogous polymer-nanoclay multilayers have also been made by a similar method [2,3]. These layer-by-layer deposition methods make use of the general concepts of electrostatic assembling and surface mediated adsorption and reaction.

Recently, several solution-based methods for synthesis of ceramic thin films [4,5] have emerged as economic alternatives to physical and chemical vapor phase deposition techniques. Amongst these methods, successive ionic layer adsorption and reaction (SILAR) [4–6] was developed (initially) for deposition of sulfide films. In the conventional SILAR method, substrates are dipped into cationic precursor solutions for adsorption of cations, rinsed to remove physisorbed cations (while chemisorbed cations remain), dipped into anionic (S^{2-}) solutions to form a monolayer or submonolayer of sulfides, and rinsed again; this four-step deposition cycle is repeated, allowing layer-by-layer growth of sulfide films.

This SILAR technique has recently been adapted to deposit oxide (e.g. ZnO, SnO_2) films from aqueous solutions [4,5], wherein a post-deposition annealing process is generally required for dehydration and crystallization of the films. Low-temperature synthesis of nanocrystalline oxide films using SILAR and a hydrothermal annealing process has been demonstrated [7]. Furthermore, a modified SILAR technique (using metal alkoxide–toluene/ethanol precursor solutions, ethanol as rising solvent, and pure H_2O for hydrolysis) has been developed for making ultrathin (1–10 nm) gate dielectric oxide (TiO_2, ZrO_2, Ta_2O_5, and La_2O_3) films [8,9]. However, the applications of these conventional SILAR techniques are generally limited by the low growth rate, i.e., ≤1 atomic layer per deposition cycle [7]. Furthermore, a requirement of thousands of dipping processes posts challenges. In general, reducing the number of dip cycles (by a factor of 10 or more) can help improving quality controls, thusly making it easier to produce thicker films while maintaining the control of uniformity and defects.

A recent letter [10] reported the preliminary feasibility of an accelerated SILAR technique without rinsing steps. In this technique, the layer-by-layer electrostatic assembling concept used for making polyelectrolyte films [1] and polymer-nanoclay

---

* Corresponding author. Tel.: +1 864 656 5961; fax: +1 864 656 1453.
E-mail addresses: jianluo@clemson.edu, jluo@alum.mit.edu (J. Luo).

0257-8972/$ - see front matter © 2007 Elsevier B.V. All rights reserved.
doi:10.1016/j.surfcoat.2007.09.041

multilayers [2,3] was adopted. This approach can be regarded as a surface precipitation process. Despite the initial success (which was largely based on one oxide system with a set of fixed deposition parameters [10]), there are critical needs to conduct a further systematic study to 1) demonstrate the tunability of the growth rate via varying the key processing parameters, 2) develop a phenomenological film growth model, and 3) verify the feasibility of this method for more than one oxide systems. This study addresses these open issues using Y_2O_3-doped ZrO_2, pure ZrO_2, and Gd_2O_3-doped CeO_2 as model systems. The major objective is to test the universality of the new deposition method and develop a model for the non-substrate-specific layer-by-layer growth rates (i.e., beyond the first layer).

Zirconia and ceria thin films have applications in fuel cells, sensors, catalysts, insulating/dielectric layers, and protective coatings. ZrO_2 and Y_2O_3-doped ZrO_2 thin films have been prepared by pulsed laser deposition (PLD) [11], sputtering [12,13], metal organic chemical vapor deposition (MOCVD) [14], and sol–gel spin coating [15,16] methods. Similarly, Gd_2O_3-doped CeO_2 thin films have been prepared by PLD [17], aerosol-assisted MOCVD [18] and sol–gel [19] methods. In addition to investigating the feasibility and film growth kinetics of this generic layer-by-layer deposition method, a secondary objective of this study is to establish a cost-effective, solution-based method for making doped zirconia and ceria thin films with high level of control.

2. Experimental procedure

Epi-polished silicon wafers with thermally oxidized surface layers (Si/SiO_2) were purchased as substrates for depositing zirconia and ceria films. These Si/SiO_2 wafers were cleaned and surface-treated following two different procedures. In an acetone cleaning procedure, the substrates were ultrasonically cleaned in acetone for 30 min and dried in air. In an alkali cleaning and surface treatment procedure, the substrates were placed in a 0.1 M NaOH solution for 20 min, neutralized in a 1 M HCl solution for 5 min, ultrasonically cleaned in distilled water for 20 min, and dried in air.

A NIMA® automatic dip coater (Nima Technology Ltd., Coventry, England) was used to deposit thin films, and the deposition processes were controlled by a personal computer with pre-set programs. The substrates were alternately dipped into cationic and anionic precursor solutions without any rinsing steps, while the dipping processes (i.e., dipping speed and holding/immersing time) were carefully controlled. The anionic precursor solution was ammonium hydroxide [$NH_4(OH)$] in distilled water, and its concentration was fixed as 1 M. Cationic precursor

Table 1
Summary of experimental conditions and measured thicknesses of as-deposited and annealed films

No. of deposition cycles	Dipping speed	Cationic concentration	Holding time	As-deposited films		Annealed films	
				Mean	Std. dev.	Mean	Std. dev.
	(mm/min)	(M)	(s)	(nm)			
ZrO_2							
10	20	0.1	45	90.0	10.7	61.0	8.7
15	20	0.1	45	125.3	8.3	85.4	9.3
20	20	0.1	45	281.1	15.0	94.3	8.0
Y_2O_3-doped ZrO_2							
Varying cationic concentration							
10	20	0.01	10	37.6	2.0	19.7	2.1
10	20	0.04	10	66.5	5.9	31.3	2.8
10	20	0.1	10	103.8	6.7	42.8	3.5
Varying dipping speed							
10	20	0.1	10	103.8	6.7	42.8	3.5
10	30	0.1	10	67.6	4.7	34.6	3.7
Varying holding time							
10	20	0.1	1	64.5	2.8	38.0	3.5
10	20	0.1	10	103.8	6.7	42.8	3.5
10	20	0.1	30	110.2	4.4	51.2	2.8
10	20	0.1	45	120.9	7.7	61.4	2.6
Varying no of deposition cycles							
5	20	0.1	45	58.6	6.4	27.6	1.6
10	20	0.1	45	120.9	7.7	61.4	2.6
15	20	0.1	45	136.9	3.7	75.8	2.3
20	20	0.1	45	181.5	16.0	110.0	10.5
Gd_2O_3-doped CeO_2							
5	20	0.1	45			37.4	8.5
10	20	0.1	45			49.1	5.5
15	20	0.1	45			75.9	14.7
20	20	0.1	45			150.3	17.1

For Y_2O_3-doped ZrO_2, the cationic concentration refers to Zr^{4+} (aq.) concentration and the Y^{3+}/Zr^{4+} ratio is kept at 0.1.

solutions of x M $Zr^{4+}+0.1x$ M Y^{3+} ($x=0.01$–0.1) were prepared from zirconyl chloride octahydrate ($ZrOCl_2 \cdot 8H_2O$) and yttrium chloride hexahydrate ($YCl_3 \cdot 6H_2O$) (Fisher Scientific, NJ) for depositing Y_2O_3-doped ZrO_2 films using a variety of different deposition parameters (Table 1). The advance and withdraw dipping speeds were controlled at either 20 or 30 mm per minute. The four dipping speeds, i.e., advance and withdraw speeds in anionic and cationic precursor solutions, were kept identical for simplicity. Specimens were held in the solutions for 1–45 s, and the holding times in anionic and cationic precursor solutions were kept identical. 5–20 deposition cycles were employed. Pure ZrO_2 films were prepared from a 0.1 M Zr^{4+} (aq.) solution. Aqueous solutions of 0.1 M $Ce^{3+}+0.01$ M Gd^{3+} were prepared from cerium nitrate hexahydrate ($Ce(NO_3)_3 \cdot 6H_2O$) and gadolinium nitrate pentahydrate ($Gd(NO_3)_3 \cdot 5H_2O$) (Fisher Scientific, NJ) for depositing Gd_2O_3-doped CeO_2 films. Ce^{3+} (aq.) solutions were used in this study because solutions of too low PH values are required to dissolve Ce^{4+} [20]; however, formation of CeO_2 films after dehydration is expected based on a prior study [20]. For making Gd_2O_3-doped CeO_2 and pure ZrO_2 films, the dipping speed and holding time, respectively, were fixed as 20 mm/min and 45 s, respectively, and films of different thickness were obtained by varying the number of deposition cycles.

As-deposited films were isothermally annealed at desired temperatures (in air) in a box furnace for 2 hours. The standard (optimized) annealing temperatures for zirconia and ceria, respectively, were 600 °C and 800 °C, respectively. The ramping and cooling rates were controlled at 5 °C per minute. Both as-deposited and annealed specimens were characterized by a field-emission scanning electron microscope (SEM, Hitachi S4800) and a variable-pressure SEM (Hitachi S3500), both equipped with energy dispersive X-ray spectroscopy (EDXS) analyzers. SEM specimens were coated with Pt/Au for increasing conductivity; alternatively, a variable-pressure SEM was employed to examine specimens without coatings. Both in-plane and cross-sectional SEM images were taken. Cross-sectional SEM specimens were made by carefully cleaving Si wafers with oxide films deposited on the surfaces, while protecting the surfaces/films with soft filter papers. Film thickness was measured from cross-sectional SEM images, and the mean and standard deviation of ten measurements made at different locations were reported for each film. For as-deposited films, some particles popped off during cleaving (for cross-sectional SEM); thus our kinetic model is derived based on the measured thicknesses of annealed films, which are more reliable. Film composition was analyzed by EDXS. Phase identification was carried out by X-ray diffraction (XRD) using a Scintag diffractometer (Cu-K_α radiation, $\lambda=1.5418$ Å, operating at 40 kV and 35A).

3. Results and discussion

3.1. Substrate preparation

SEM images of Y_2O_3-doped ZrO_2 films deposited on acetone cleaned substrates and alkali cleaned and treated substrates show a significant difference in crack formation (Fig. 1). The thin films deposited on alkali cleaned and treated substrates are essentially crack-free. However, the simple acetone cleaning procedure does not appear to be aggressive enough, where the observed cracks (Fig. 1a) presumably nucleated around the remaining dust particles or other contaminations. These results illustrate that sufficient cleaning of the substrate and proper surface treatment prior to the deposition are essential for making uniform and crack-free films. It should be emphasized that the defect formation and density should always depend on the cleanness of the production environment and the effective surface cleaning/treatment method should be chosen specifically for a particular substrate. Further optimization should be conducted independently for specific substrates/materials and production environments, which is beyond the scope of this study. The alkali cleaning procedure used in this study is standard and well-characterized cleaning procedure for glass surfaces (or Si/SiO_2 where the surface is amorphous SiO_2) [21]; it is well known that NaOH lightly etches SiO_2 and therefore ensures the removal of all surface residues and a subsequent short dip in HCl solution neutralizes the surface; after additional water rinsing, clean surfaces are expected from extensive prior studies [21] and evident by the observation of essentially crack-free films in this study. The alkali cleaning and surface treatment procedure was used for the rest of this study.

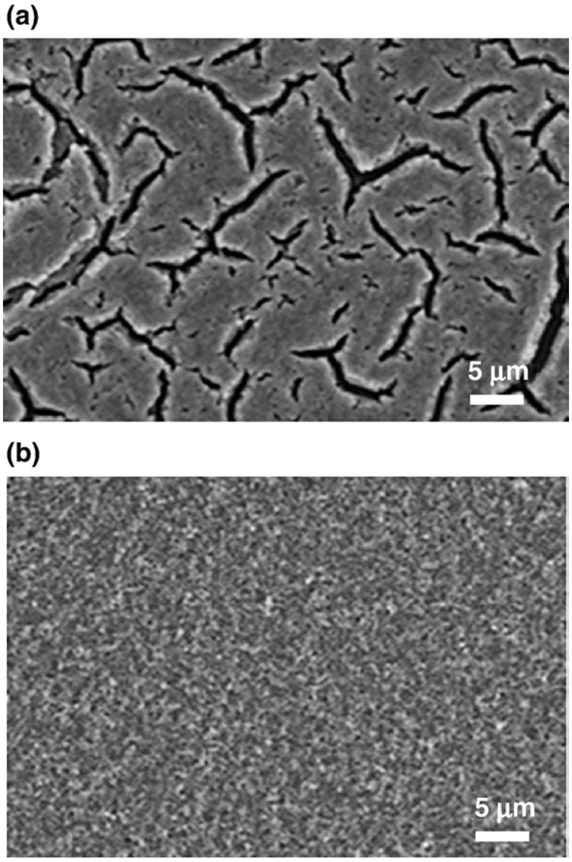

Fig. 1. SEM images of Y_2O_3-doped ZrO_2 films deposited on (a) acetone and (b) alkali cleaned substrates. These results illustrate that sufficient cleaning of the substrate and proper surface treatment are essential for making crack-free films, although the optimal cleaning and surface treatment method should be substrate/material specific.

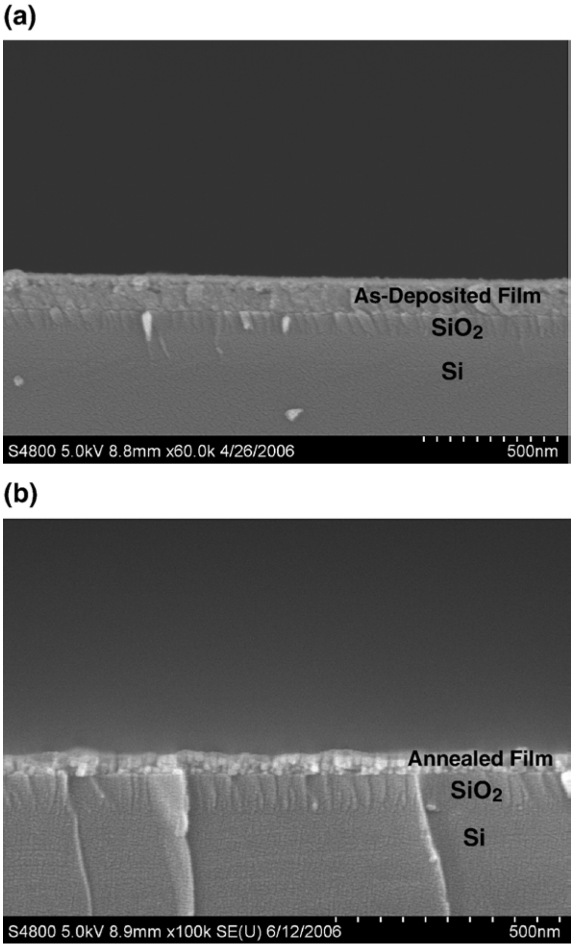

Fig. 2. Cross-sectional SEM images of (a) as-deposited and (b) annealed Y_2O_3-doped ZrO_2 films. The specimen shown in (b) was annealed at 600 °C for 2 hours.

3.2. Film characterization

Figs. 2 and 3 are cross-sectional SEM image of as-deposited and annealed Y_2O_3-doped ZrO_2 and Gd_2O_3-doped CeO_2 thin films. As-deposited hydroxylated films are highly uniform in thickness (Figs. 2a and 3a). Some roughness has been introduced by the thermal annealing process (Figs. 2b and 3b), which can be further improved via (independently) optimization of the thermal annealing process or introducing of a hydrothermal annealing process [7]. The annealed films are nanocrystalline; nano-sized grains can be seen in the SEM images shown in Figs. 2b and 3b and broadening of XRD peaks due to the small grain sizes is also evident in Fig. 4. Some decohesion has been observed for as-deposited Gd_2O_3-doped CeO_2 thin films, which presumably occurred during SEM specimen preparation (cleave of the wafers) as a result of low adhesion between the as-deposited films and the Si/SiO_2 substrates. Due to low adhesion, films or part of films often fall off or even shatter when the specimens were cleaved for SEM cross-sectional characterization; thus it is difficult to reliably measure the thickness of as-deposited (hydrated) CeO_2-Gd_2O_3 films. Thus, these thickness values are not reported in Table 1. Decohesion was not observed for annealed Gd_2O_3-doped CeO_2, showing increasing adhesion after 800 °C annealing. Decohesion was not observed for any of the as-deposited and annealed zirconia films.

XRD patterns are shown in Fig. 4. The XRD pattern of an Y_2O_3-doped ZrO_2 specimen annealed at 600 °C matches that of tetragonal or cubic phase of yttria-stabilized zirconia (Fig. 4a) [10]. When the annealing temperature is increased to 800 °C, minor monoclinic phase precipitated (Fig. 4b). Gd_2O_3-doped CeO_2 thin films are rather poorly crystallized even after annealing at 800 °C (Fig. 4c). Nonetheless, the XRD pattern appears to match that of the CeO_2 cubic phase, which is consistent with the prior observation that CeO_2 formed after dehydration [20]. EDXS compositional analysis confirmed the presence of yttrium in the Y_2O_3-doped ZrO_2 films, but quantitative analysis could not be conducted for this system due the partial overlaps of Y and Zr peaks and the rather weak signals from thin films. Quantitative EDXS film composition analysis has been conducted for Gd_2O_3-doped CeO_2 thin films; the measured Gd/Ce atomic ratio is ~0.13, which agrees well with the cation ratio in the precursor solution (=0.1).

3.3. Film thickness versus number of deposition cycles

Fig. 5 shows thickness versus the number of deposition cycles for annealed Y_2O_3-doped ZrO_2 (YDZ), pure ZrO_2, and Gd_2O_3-doped CeO_2 (GDC). The measured film thicknesses and

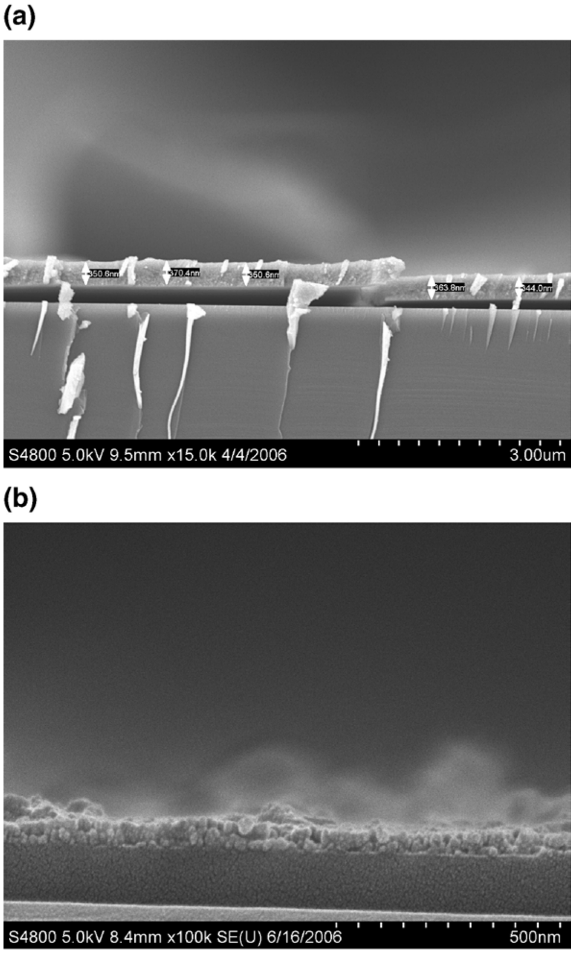

Fig. 3. Cross-sectional SEM images of (a) as-deposited and (b) annealed Gd_2O_3-doped CeO_2 films. The specimen shown in (b) was annealed at 800 °C for 2 hours.

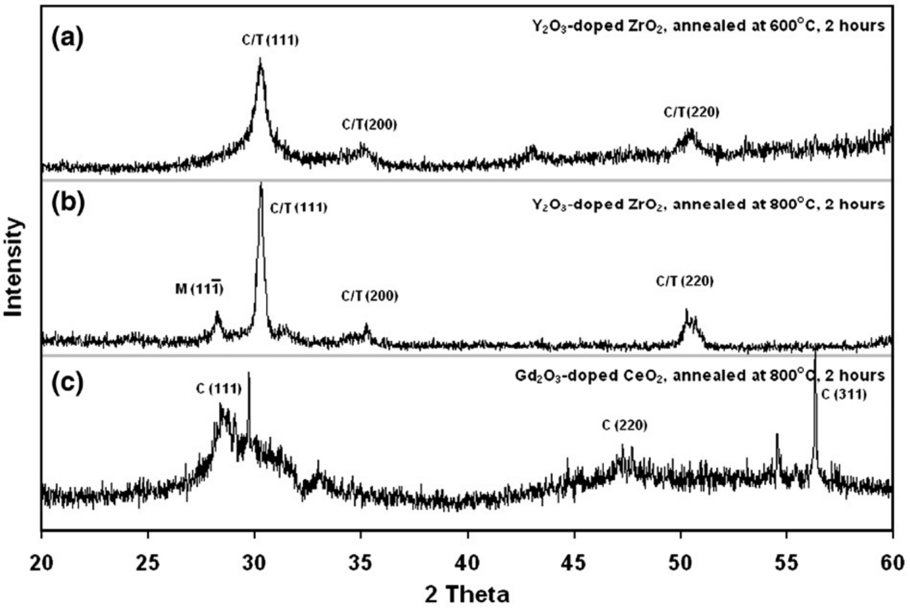

Fig. 4. XRD patterns of annealed films. Panel (a) is from Ref. [10] and included for comparison. The labels C, T, and M refer to the cubic, tetragonal or monoclinic phases, respectively.

associated experimental conditions are listed in Table 1. For all three systems, film thickness increases monotonically with increasing number of deposition cycles. Linear fits for these three set of data are also shown in Fig. 5. The equivalent "growth rates" for annealed oxide films are found to be ~5.4 nm/cycle for Y_2O_3-doped ZrO_2, ~5.2 nm/cycle for pure ZrO_2, and ~6.4 nm/cycle for Gd_2O_3-doped CeO_2, respectively, for films that were made using the following deposition parameters: 0.1 M nominal cationic concentration; 20 mm/min dipping speed; and 45 s holding time.

These film growth rates are >10 times greater than the conventional SILAR method for ZrO_2 films [7]. No significant dissolution back of the Gd_2O_3-doped CeO_2 films was evident in this study (at least for preparing up to ~150 nm thick annealed films; see Fig. 5), although this was reported as an issue for preparing Sm-doped CeO_2 via the conventional SILAR method [20]. Based on SEM images (Fig. 3), these doped CeO_2 films made in this study appear to be significantly more uniform than those Sm-doped CeO_2 made by the conventional SILAR method [20], though the specific effects of deposition environments (cleanness) and substrates are unknown for making a more critical comparison of the effectiveness of these method in making uniform films.

3.4. Tunable growth rate and phenomenological film growth model

A focus of this study is to investigate the effects of various deposition parameters on film growth rate, thereby demonstrating the tunability of the growth rate and establishing a film growth model. In this modified SILAR method, layer-by-layer growth of uniform film is presumably mediated by electrostatic assembling and surface precipitation reaction, akin to those assumed for layer-by-layer deposition of polyelectrolyte multilayers [1]. Thus, unlike the convention SILAR wherein the film growth is thermodynamically controlled (which is largely independent of the dipping speed and holding time; therefore the control of the dipping process is unimportant) [4–6], film growth in this modified SILAR process can be limited by either the surface reaction kinetics or the mass transfer in the solution. Consequently, the growth rate is tunable via changing the key processing parameters such as the dipping speed and holding/immersing time as well as the concentrations of the precursor solutions, which is clearly demonstrated in Fig. 6a–c. The measured film thicknesses and standard deviations are listed in Table 1.

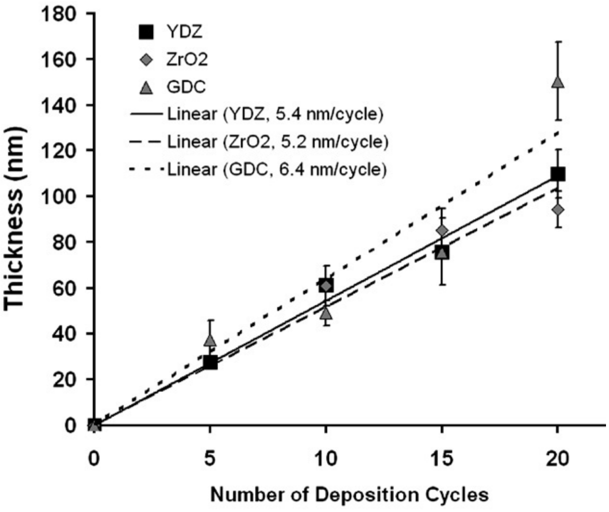

Fig. 5. Thickness versus number of deposition cycles for annealed films. Errors bars represent ±1 standard deviations. Lines represent the best linear fits. The YDZ data are from Ref. [10] and included for comparison. Detailed deposition parameters and measured thicknesses are listed in Table 1.

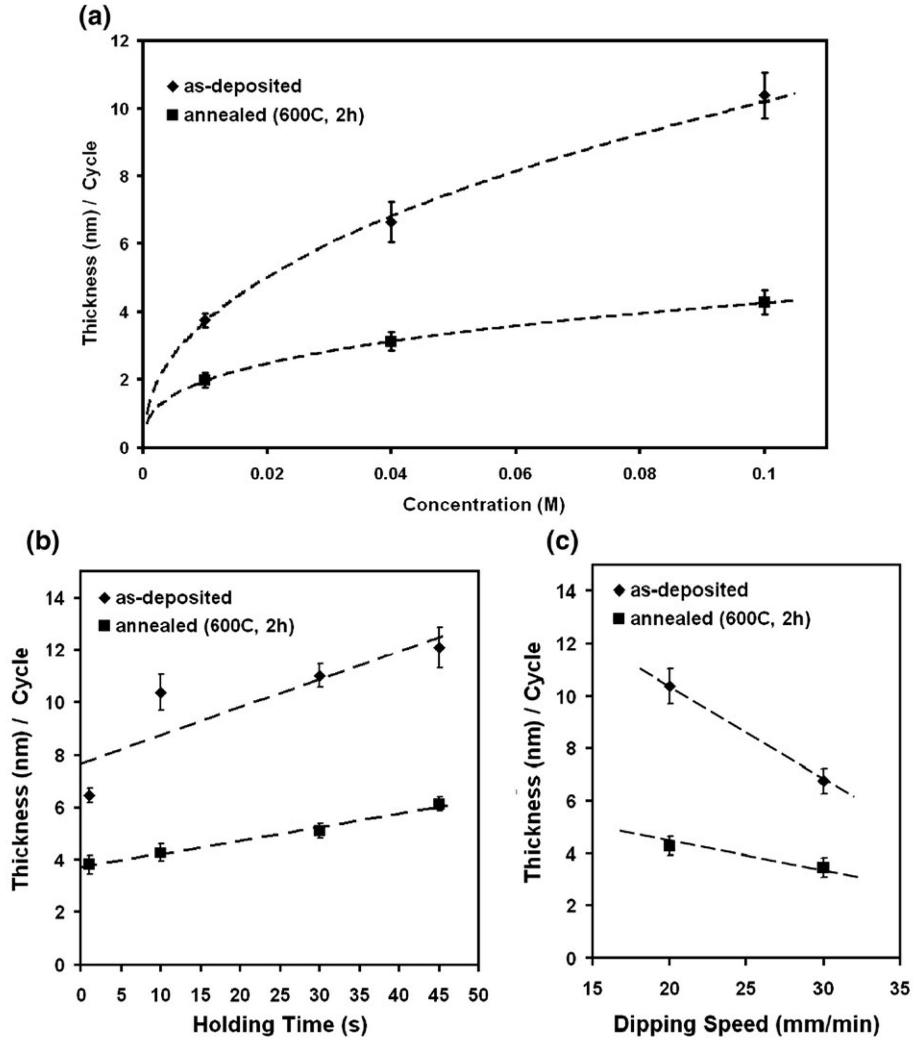

Fig. 6. Film thickness per deposition cycle versus (a) cationic solution concentration, (b) holding time, and (c) dipping speed. Error bars represent ± 1 standard deviations. Detailed deposition parameters and measured thicknesses are listed in Table 1.

It is important to point out that the error bars in Figs. 5 and 6 represent the standard deviations of ten thickness measurements, which were made typically in two SEM images (i.e., five measurements along the surface with 200–300 nm intervals in each SEM image). Thus, these error bars represent the film uniformity at a small length scale (~100 nm to ~1 µm) and likely underestimate the real errors, which should also include the large length scale roughness in film thickness (from ~1 µm to >1 cm) as well as the additional errors caused by the falling of the particles during cleaving the specimens for SEM cross-sectional examination (which is a particular concern for as-deposited films). These are due to intrinsic limitations for measuring film thickness in SEM cross-sectional images.

Fig. 6a clearly shows that the film growth rate, which is measured by thickness per deposition cycle, depends on the concentration of the cationic precursor solution. When the concentration decreases from 0.1 M to 0.01 M, the observed growth rate decreases monotonically from ~4.3 (~10) to ~2.0 (~3.8) nm/cycle for annealed (as-deposited) films. In other words, the film growth rate is reduced by ~50–60% for a 10-fold reduction in the cationic precursor solution concentration. This observation is expected since the deposition rate should decrease monotonically with decreasing solution concentration and approach zero as the cationic concentration is reduced to zero.

Growth rate versus holding (immersing) time in cationic/anionic precursor solutions is shown in Fig. 6b. With increasing holding time from 1 s to 45 s, the growth rate increases almost linearly from ~3.8 (~6.5) to ~6.1 (~12) nm/cycle for annealed films (The measured thicknesses of annealed films, which are more reliable, are used for building the film growth model; see the "Experimental procedure" section). To the first order of approximation, it can be reasonably assumed that the growth rate (dh/dn) linearly depends on the holding time (t_{holding}):

$$\frac{dh}{dn} = a(c,v) + b(c) \cdot t_{\text{holding}} + \mathrm{O}\left(t_{\text{holding}^2}\right). \tag{1}$$

In Eq. (1), $a(c,v)$ and $b(c)$ are parameters that depend on the solution concentration (c) and dipping speed (v). (In a more general case, these constants should depend on both cationic and anionic precursor solution concentrations as well as four advance/withdraw dipping speeds. For simplicity, the anionic concentration was fixed, and the all dipping speeds were kept identical in this study.)

A physical explanation of Eq. (1) is given as follows: $a(c,v)$ represent the growth rate (per cycle) during the dipping with zero holding time and $b(c)$ represents the additional growth rate (per cycle per unit time) during holding (the overall effects of the two dips within a cycle). It should be noted that the conditions and extent of a linear relation are somewhat uncertain (the slope of thickness versus holding time for annealed films in Fig. 1b is small; thus the correlation is less significant for given errors). On the other hand, the data for as-deposited films seems to suggest a fast initial increase with holding time which levels off for longer time. Thus, the existence of this linear regime in Fig. 6(b) is not fully supported. Nonetheless, film thickness should monotonically increase with holding time and a linear relation may be used as a first-order approximation (in a Taylor series as shown in Eq. (1)). Then, an empirical fitting of the measured thickness (of the annealed films) versus holding time (Fig. 6b) to Eq. (1) produces:

$$\begin{cases} a(0.1\ M,\ 20\ \mathrm{mm/min}) = 3.73\ \mathrm{nm/cycle} \\ b(0.1\ \mathrm{M}) = 0.052\ \mathrm{nm/cycle/sec} \end{cases} \quad (2)$$

The correlation coefficient for this linear regression was calculated to be $R^2=0.9892$ or $R=0.9945$.

Furthermore, when the dipping speed increases from 20 to 30 mm/min, the growth rate decreases from ~4.3 (~10) to ~3.5 (~6.8) nm/cycle for annealed (as-deposited) films (Fig. 6c). Presumably, the reaction time is less with a higher dipping speed, resulting in a thinner film, consistent with the trend shown in Fig. 6c. However, a critical assessment for film growth rate as a function of dipping speed is not feasible given the limited range of tested dipping speeds and the weak dependence of film growth rate on dipping speed as shown in Fig. 6c. Furthermore, the growth rate difference for films prepared by two dipping speeds as shown in Fig. 6c is barely beyond experimental errors (especially for the case of annealed specimens). Nonetheless, a rough estimation can be made from Eqs. (1) and (2):

$$a(0.1\ \mathrm{M},\ 30\ \mathrm{mm/min}) = 2.96\ \mathrm{nm/cycle}. \quad (3)$$

Intuitively, it may be expected that $a(c_0,v)$ increases monotonically with $1/v$ (which scales with the “equivalent reaction time” during the dipping process) when the solution concentrations are all fixed. Theoretically,

$$a(c_0, v \rightarrow +\infty) \rightarrow 0. \quad (4)$$

Thus, $a(c_0,v)$ can be expanded as a power series of $1/v$, where the constant term is zero. To the first order of approximation, it may be assumed that $a(c_0,v)$ is proportional to $1/v$, but this linear approximation is not generally held at typical film deposition conditions. In this particular case,

$$\frac{a(0.1\ \mathrm{M}, v_1)}{a(0.1\ \mathrm{M}, v_2)} = \frac{3.73\ \mathrm{nm/cycle}}{2.96\ \mathrm{nm/cycle}} \approx 1.26 < \frac{1/v_1}{1/v_2} = \frac{v_2}{v_1} = \frac{30\ \mathrm{mm/min}}{20\ \mathrm{mm/min}} = 1.5, \quad (5)$$

This indicates that film growth during this dipping process is beyond the linear regime and the coefficient for the parabolic term is likely negative, or

$$\frac{d^2[a(c,v)]}{d[1/v]^2} < 0. \quad (6)$$

It is expected that both $a(c,v)$ and $b(c)$ increase with increasing solution concentration, which is clearly evident in Fig. 6a. The specific functional dependence on solution concentration(s) can be complex and is presumably related to the equilibrium ionic adsorption profile at solution/substrate interfaces (which is described by the electrical double-layer theory and other related models [22]). However, a pure thermodynamic theory is not sufficient and kinetics of surface and electrostatic mediated precipitation and the mass transfer rates in the solutions must be taken into consideration. Although in gas-phase deposition processes, the regimes controlled by surface reaction kinetics and by mass transfer are often distinct, these regimes may not be clearly separable in a SILAR-like solution based processes.

A more critical assessment is not warranted at this point. Nonetheless, Fig. 6a–c and the above discussion clearly demonstrate that 1) the film growth is controlled by surface reaction kinetics and/or mass transfer in solutions, 2) the growth rate can be systematically tuned by varying several key deposition parameters, and 3) the observed general trends can be explained from a (preliminary) phenomenological film growth model.

4. Concluding remarks

The feasibility of a novel yet simple layer-by-layer deposition method for preparing oxide thin films from aqueous solutions have been studied using Y_2O_3-doped ZrO_2, pure ZrO_2, and Gd_2O_3-doped CeO_2 as model systems. A phenomenological film growth model is proposed. An alkali cleaning and surface treatment procedure has been found to be rather effective for making uniform and crack-free films on Si/SiO_2 substrates. The film thickness increases linearly with the number of deposition cycles, and a constant growth rate for a given set of deposition parameters (on the order of a few nanometers per deposition cycle) is demonstrated. The film growth is kinetically controlled and the growth rate is tunable via changing several key kinetic parameters and solution concentrations. This deposition technique can be adapted for making other oxide films and combined with a hydrothermal dehydration process [7] for making high-quality nanocrystalline films at even lower temperatures. The film growth rate is significant and tunable, making this a viable and economic oxide film deposition technique. The defect formation control and the effective surface treatment method should be independently optimized for specific substrates and production environments.

The success of this study enables further endeavors to make a variety of novel oxide-based nanostructured films. This layer-by-layer deposition technique can be conveniently adapted for making periodic multilayers or functionally-graded oxide films via changing the composition or concentration of cationic precursor solutions periodically or continuously.

This research was supported in part by a research initiation grant from South Carolina Space Grant Consortium, a NASA/SC EPSCoR grant via University of South Carolina, and a National Science Foundation CAREER award (DMR-0448879). We thank A. Kumbhar, Dr. J. Hudson and D. Cash for assistance in using SEM, and Dr. J. Sanders for assistance in using XRD. We acknowledge three anonymous reviewers for their insightful comments.

References

[1] P.T. Hammond, Advanced Materials 16 (2005) 1271.
[2] M. Rubner, Nature 423 (2003) 925.
[3] Z. Tang, N.A. Kotov, S. Magonov, B. Ozturk, Nat. Mater. 2 (2003) 413.
[4] T.P. Niesen, M.E.D. Guire, J. Electroceramics 6 (2001) 169.
[5] T.P. Niesen, M.E.D. Guire, Solid State Ionics 151 (2002) 61.
[6] Y.F. Nicolau, Appl. Surf. Sci. 22/23 (1985) 1061.
[7] S. Park, B.L. Clark, D.A. Keszler, J.P. Bender, J.F. Wager, T.A. Reynolds, G.S. Herman, Science 297 (2002) 65.
[8] Y. Aoki, T. Kunitake, Advanced Materials 16 (2004) 118.
[9] Y. Aoki, T. Kunitake, A. Nakao, Chem. Mater. 17 (2005) 450.
[10] P.K. Arcot, J. Luo, Mater. Lett., doi:10.1016/j.matlet.2007.04.078 (in press).
[11] A.P. Caricato, A.D. Cristoforo, M. Fernandez, G. Leggieri, A. Luches, G. Majni, M. Martino, P. Mengucci, Appl. Surf. Sci. 208–209 (2003) 615.
[12] T. Hata, K. Sasaki, Y. Ichikawa, K. Sasaki, Vacuum 59 (2000) 381.
[13] S.H. Jeong, I.S. Bae, Y.S. Shin, S.B. Lee, H.T. Kwak, J.H. Boo, Thin Solid Films 475 (2005) 354.
[14] S.-Y. Chun, N. Mizutani, Appl. Surf. Sci. 171 (2001) 82.
[15] Y. Zhang, S. Jin, C. Liao, C.H. Yan, Mater. Lett. 56 (2002) 1030.
[16] Q. Zhang, X. Li, J. Shen, G. Wu, J. Wang, L. Chen, Mater. Lett. 45 (2000) 311.
[17] L. Chen, C.L. Chen, D.X. Huang, Y. Lin, X. Chen, A.J. Jacobson, Solid State Ionics 175 (2004) 103.
[18] H.Z. Song, H.B. Wang, S.W. Zha, D.K. Peng, G.Y. Meng, Solid State Ionics 156 (2003) 249.
[19] C. Xia, Y. Zhang, M. Liu, Electrochem. Solid-State Lett. 6 (2003) A290.
[20] S. Park, G.S. Herman, D.A. Keszler, J. Solid State Chem. 175 (2003) 84.
[21] J. Livage, in: M.A. Aegerter, M. Mennig (Eds.), Sol–Gel Technologies for Glass Producers and Users, Kluwer Academic Publishers, Boston, 2004, p. 29.
[22] J.N. Israelachvili, Intermolecular and Surface Forces, Academic Press Limited, London, 1994.